Journal of Physics and Chemistry of Solids 73 (2012) 554–558

Contents lists available at SciVerse ScienceDirect

Journal of Physics and Chemistry of Solids

journal homepage: www.elsevier.com/locate/jpcs

High hardness, low Young's modulus and low friction of nanocrystalline ZrW_2 Laves phase and $Zr_{1-x}W_x$ thin films

D. Horwat [a,*], E. Jimenez-Pique [b,c], J.F. Pierson [a], S. Migot [a], M. Dehmas [d], M. Anglada [b,c]

[a] Institut Jean Lamour, Département CP2S, UMR 7198 CNRS-Nancy-Université-UPV-Metz, Ecole des Mines de Nancy, Parc de Saurupt, CS14234, 54042 Nancy, France
[b] Department of Ciencia de Materiales e Ingeniería Metalúrgica, Universitat Politècnica de Catalunya, Avda. Diagonal 647 (ETSEIB), 08028 Barcelona, Spain
[c] Center for Research in Nanoengineering, Universitat Politècnica de Catalunya, C/Pascual i Vila, 15, 08028 Barcelona Spain
[d] Institut Jean Lamour, Département SI2M, UMR 7198 CNRS-Nancy-Université-UPV-Metz, Ecole des Mines de Nancy, Parc de Saurupt, CS14234, 54042 Nancy, France

ARTICLE INFO

Article history:
Received 18 August 2011
Received in revised form
1 December 2011
Accepted 14 December 2011
Available online 22 December 2011

Keywords:
A. Intermetallic compounds
A. Nanostructures
A. Thin films
D. Mechanical properties

ABSTRACT

$Zr_{1-x}W_x$ nanocrystalline films of Zr-W solid solutions and ZrW_2 Laves phase were synthesized by magnetron co-sputtering. Large values of the *H/E* ratio up to 0.09 are observed for grain sizes in the nanometer range along with a hardness above 10 GPa and Young's modulus below 230 GPa. *H/E* values are correlated with the developed surface of grain boundaries suggesting an elastic deformation mostly handled by the grain boundaries. This is associated to friction coefficients comparable to those of metallic glass surfaces. In contrast to fragile bulk Laves phases, no cracks were detected at the film surface after indentation and scratch test of nanocrystalline ZrW_2. The friction coefficient of such films against diamond tip was in the range 0.08–0.15, similarly to metallic glass surfaces.

1. Introduction

Nanostructured thin films offer outstanding mechanical features relative to single phase materials (see for instance the comprehensive review of Meyers et al. [1]). Extremely fine grained structure allow taking the best profit of the Hall-Petch hardening [2]. The additional presence of an amorphous phase surrounding the nanocrystals is supposed to toughen the material by blocking the motion of dislocations and disabling crack propagation. In very fine grain nanocrystalline films the amorphous phase can either be of different chemical nature from the crystals or constituted by the grain boundaries. Such arrangements were successfully exploited and extensively studied in order to design relatively tough super-hard and ultra-hard ceramic–ceramic nanocomposites [3–5]. Although they seem to break the law of compromise, ceramic–ceramic nanocomposites remain rather brittle. Metal–metal systems are in essence softer but less brittle than their ceramic–ceramic counterpart. They are particularly interesting due to a high hardness *H* achieved through Hall-Petch hardening while keeping an elastic modulus *E* characteristic of metals. This is a powerful strategy to significantly improve the *H/E* ratio, a parameter known to drive the friction behavior of materials [6,7]. Despite these potential advantages few studies relied on the mechanical characterization of metal–metal nanocomposites. Recently, hardness and *H/E* data in the 2–4 GPa and 0.02–0.04 ranges were, respectively, reported in Cu_xAg_{1-x} nanostructured thin films [8]. Despite a sensitive enhancement of the mechanical properties compared to the bulk properties, the inherent softness of Cu and Ag prevent achieving high hardness and *H/E* ratio. Sputter-deposited Zr-based binary alloys may be considered due to their good ability to form nanostructures [9–13]. We observed recently the formation of nanostructures with grain sizes ranging from 1.3 to 16 nm in thin films of the $Zr_{1-x}W_{1-x}$ system [13]. Other authors reported a high corrosion resistance in acidic media for XRD amorphous thin films of the same system [14]. The incorporation of W into Zr implies good elastic properties because W is the transition metal exhibiting the highest valence bond [15] known to directly impact on the cohesive energy [16,17]. In addition, the Zr-W system exhibits a topologically compact intermetallic phase ZrW_2. ZrW_2 belongs to AB2 Laves phases where A and B are transition metals. Laves phase are considered for many practical applications but suffer from a low ductility and brittle fracture characteristics at ambient temperatures [18]. Therefore, there is a great deal of interest in improving the ductility of Laves phases around ambient temperatures (see for instance [18–20]). The motivation of this paper is to highlight the mechanical features of $Zr_{1-x}W_x$ ($x=0.43$–0.81) thin films condensed from a magnetron sputtering vapor.

2. Experimental setup

$Zr_{1-x}W_x$ films were deposited on glass substrates by co-sputtering of Zr and W metallic targets in the presence of

* Corresponding author. Tel.: +33 3 83 58 42 52.
E-mail address: david.horwat@ijl.nancy-universite.fr (D. Horwat).

0022-3697/$ - see front matter © 2011 Elsevier Ltd. All rights reserved.
doi:10.1016/j.jpcs.2011.12.009

argon. The experimental device is a 40-L sputtering chamber pumped down via a mechanical and a turbo-molecular pump allowing a base vacuum of 10^{-4} Pa. It is equipped with two targets mounted on unbalanced magnetrons with their axis separated from 120 mm each other. The substrates are placed next to the magnetron axis on a rotating substrate holder parallel to the target surfaces. The distance between the glass substrates and the target surface was fixed at 50 mm. The zirconium target (50 mm diameter, 3 mm thick and purity higher than 99.9%) was powered by an Advanced Energy Pinnacle +5 kW DC pulsed generator. The discharge frequency was fixed at 50 kHz and the off-time was fixed at 4 μs. The current applied to the zirconium target (I_{Zr}) was kept constant at 0.3 A. The tungsten target, 50 mm in diameter, 3 mm-thick and purity higher than 99.9%, was powered by an Advanced Energy MDX 1.5 kW DC generator. The current applied to the tungsten target (I_W) was ranging between 0 and 0.7 A. The argon flow rate was regulated at 20 sccm using an MKS flow meter. Within these deposition conditions, the working pressure measured using an MKS Baratron absolute gage was close to 0.25 Pa. The deposition duration was fixed at 20 min. $Zr_{1-x}W_x$ films were deposited without external heating and the deposition temperature was close to 50 °C. The chemical analyses were carried out by electron probe microanalysis (EPMA) using a Cameca SX50 electron microprobe. The composition was deduced from the average of ten measurements for each sample. The absolute error is in the range ±0.1 at.%. X-ray diffraction (XRD) measurements were conducted in glancing angle conditions with K_αCo radiation (λ=0.178897 nm) and an incident angle of 4° using an INEL diffractometer. Transmission electron microscopy (TEM) investigations were performed using a Philips CM200 microscope. Indentations were done using a MTS Nanoindenter XP equipped with continuous stiffness measurement module (CSM), which allows a continuous capture of the stiffness of the material during the loading part. The experiments were performed with a diamond Berkovich indenter tip with its function area calibrated against fused silica standard. Strain rate was set constant and equal to 0.05 s^{-1}. Poisson ratio was taken equal to 0.25. Nine to twelve measurements were made and averaged. Young's modulus E and hardness H were calculated with the Oliver and Pharr method [21–23]. Maximum indentation depths were 500 nm and 1000 nm, although data of hardness and Young's modulus were calculated with the CSM stiffness channel, so values were obtained for all penetration depths. Hardness of the coating was obtained directly from the results at low penetration depths, were the influence of the substrate is negligible (Buckle criterion of 10%). In order to calculate the Young's modulus of the different films, the thin film model proposed by Saha and Nix [24] was used. Other thin film models [25,26] yielded comparable results. Scratch tests were performed by the same instrument, recording lateral force during scratch in order to obtain the friction coefficient.

3. Results and discussion

The elaboration conditions and mechanical properties of the synthesized films are summarized in Table 1. By changing the current I_w applied to the tungsten target it was possible to synthesize $Zr_{1-x}W_{1-x}$ films with x in the 0.43–0.81 range. I_w was carefully set in the 0.3–0.4 A range in order to investigate precisely the properties of thin films with a composition close to that of ZrW_2. Fig. 1 highlights the structural characteristics as investigated by X-ray diffraction. The XRD diffractograms of samples G and H exhibit well defined diffraction peaks, which were ascribed to the bcc lattice of tungsten in which zirconium atoms partially substitute tungsten. The cell parameters

Table 1
Some properties of the synthesized $Zr_{1-x}Wx$ films as a function of the current applied to the tungsten target. hcp: hexagonal close packed, fcc: face centered cubic, bcc: body centered cubic, ss: solid solution. *The precision is better than 5% and 10% for H and E, respectively.

Sample	Thickness (nm)	W content (at.%)	Structure	Grain size (nm)	H (GPa)*	E (GPa)*	H/E
A	480	43	Zr(W)	1.4	10	110	0.091
B	825	64	ZrW_2 in a-matrix	1.2	11.8	123	0.096
C	760	65.8	ZrW_2 in a-matrix	1.3	11.5	132	0.087
D	625	67.5	ZrW_2	1.4	10	117	0.085
E	700	69	ZrW_2	1.3	11	126	0.087
F	700	71.6	W(Zr)	1.4	11	125	0.088
G	790	76.2	W(Zr)	13.7	15	190	0.079
H	950	80.9	W(Zr)	15.9	15	230	0.065

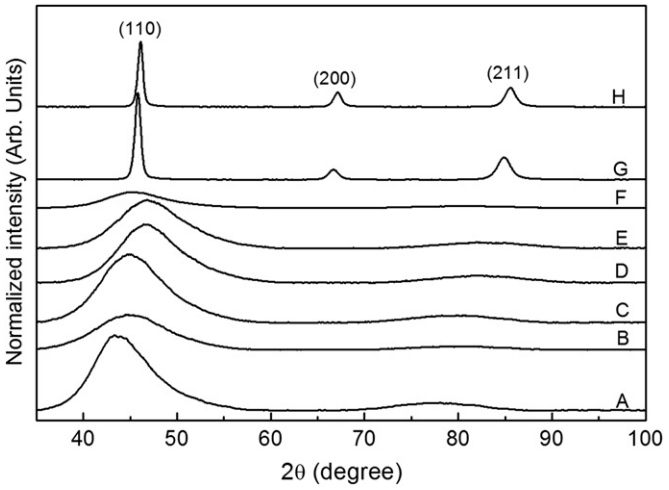

Fig. 1. Glancing angle X-ray diffractograms of $Zr_{1-x}W_x$ thin films.

estimated from the (200) diffraction peak are approx. 3.25 nm and 3.23 nm for samples G and H, respectively, against 3.18 nm reported for pure tungsten. The average crystal size of the coatings was estimated, by applying the Scherrer formula [27], to 14 for sample G and 16 nm for sample H. In contrast, broad diffraction features are observed on the XRD diffractograms of samples A to F. As the main diffraction line is very broad, the average grain size can be calculated with a good accuracy and is found below 1.5 nm. For a deeper insight into the microstructure, samples A to F were analyzed by TEM. Fig. 2 displays selected area electron diffraction (SAED) patterns and dark field images of samples A and F. The SAED pattern of sample A shows broad diffraction rings, which is typical for nanocrystalline materials. The rings were indexed as the diffraction features of a supersaturated solid solution of nanocrystalline hexagonal close packed zirconium substituted by approx. 40 at% of tungsten. This is in line with the tungsten content for this sample (see Table 1). The dark field image corresponding to a selected zone of the (100) ring evidences small crystallites with a diameter close to 1 nm, in good agreement with the XRD analysis. The composition of samples B to F (x=0.64–0.72) is close to that of ZrW_2 the only intermetallic phase reported in the Zr-W system [28]. The SAED pattern and associated dark field image of sample F are typical for the results obtained for thin films of these compositions (samples A-F). The broad rings of the SAED pattern were indexed in reference to the theoretical diffraction features of the ZrW_2 Laves phase with $Fd\bar{3}m$space group. As for sample A the dark field image evidences